Full spin-orbit coefficient in III-V semiconductor wires based on the anisotropy of weak localization under in-plane magnetic field

Toshimichi Nishimura,[1,*] Kohei Yoshizumi,[1,*] Takahito Saito,[1] Daisuke Iizasa,[1] Junsaku Nitta,[1,2,3] and Makoto Kohda[1,2,3,4,†]

[1]*Department of Materials Science, Graduate School of Engineering, Tohoku University, Sendai 980-8579, Japan*

[2]*Center of Spintronics Research Network, Tohoku University, Sendai 980-8577, Japan*

[3]*Center of Science and Innovation in Spintronics (Core Research Cluster), Tohoku University, Sendai 980-8577, Japan*

[4]*Division for the Establishment of Frontier Sciences of the Organization for Advanced Studies, Tohoku University, Sendai 980-8577, Japan*

(Received 2 October 2020; revised 26 January 2021; accepted 10 February 2021; published 8 March 2021)

Because of the one-dimensional confinement of electron momentum in narrow semiconductor wires, spin relaxation is suppressed irrespective of the presence of spin-orbit (SO) interaction. In quantum transport, weak localization corrections to conductivity are reflected as suppressed spin relaxation, which makes quantification of the SO strength difficult because quantum correction theory requires weak antilocalization when evaluating SO coefficients. Narrow wires with strong SO interaction are potential platform for Majorana particles and parafermions for topological electronics and quantum computation, so revealing the SO strength in semiconductor wire structures is beneficial. Herein, we present quantification of the full SO coefficient under weak localization in InGaAs-based narrow wires. Using anisotropic weak localization observed under an in-plane external magnetic field with various orientations, one can ascertain the relative ratio between Rashba (α) and linear Dresselhaus (β_1) SO coefficients with no fitting. Furthermore, we find that widely tuning the potential profile of the quantum well through the top gate can expose a Rashba-predominant region in magnetoconductance, where the α value can be extracted reliably from two-dimensional quantum correction theory. Finally, we quantify the full SO coefficients including Rashba, linear Dresselhaus, and cubic Dresselhaus terms in the wire.

DOI: 10.1103/PhysRevB.103.094412

I. INTRODUCTION

Spin-orbit (SO) interaction plays a crucially important role for various phenomena in condensed matter physics such as the persistent spin helix state [1–6], persistent skyrmion lattices [7], exotic quasiparticles [8,9], topological superconductivity [10], and the vanishing of interband absorption for light propagation [11]. In a III-V semiconductor quantum well (QW), the breaking of structural and bulk inversion symmetry induces Rashba [12] and Dresselhaus [13] SO interactions, which exhibit different effective magnetic field symmetries respectively in electron momentum space. As the orientation of SO-induced effective magnetic field becomes momentum dependent, electron scattering randomizes the spin precession axis, thereby resulting in D'yakonov-Perel' spin relaxation [14]. Using quantum transport, the spin relaxation induced by SO effective fields can be probed sensitively through the weak antilocalization (WAL) correction in conductivity [15,16]. Development of the quantum correction theory to conductivity enables us to quantify the SO strength including the Rashba α, linear β_1, and cubic β_3 Dresselhaus coefficients from magnetotransport experiments [16–29]. However, one must rely on different quantum correction models depending on whether the transport regime is diffusive or ballistic [16,20,22,23], and the relative strength between Rashba and Dresselhaus SO interactions [16–19,22,23–29]. Recent progress of the quantum correction contributes to the evaluation of arbitrary Rashba and Dresselhaus SO strengths [25–29]. In all existing models, precise determination of the SO strength predominantly requires WAL corrections to the conductivity because the induced spin phase is susceptible to momentum-dependent SO fields. When spin relaxation is suppressed or minimized, the lack of spin phase shift for the electron waves engenders constructive interference, resulting in weak localization (WL) corrections to the conductivity. Consequently, precise evaluation of SO strength in the existing quantum correction theory becomes difficult because it relies on WAL corrections.

The situation for suppressed spin relaxation in the presence of SO interaction is particularly beneficial for spintronics and quantum information technology because one can preserve spin information for a long time while simultaneously manipulating the spin state with the SO field. Nevertheless, achieving these benefits poses challenges because the SO interaction becomes a double-edged sword to the spin relaxation and the spin manipulation: it can randomize or control the spin phase. When the Rashba and linear Dresselhaus SO interactions are of equal strength, then spin SU(2) symmetry is preserved [2], i.e., invariance arises with respect to the specific rotations of electron spins. This invariance leads to the suppression of spin relaxation, although the spin phase is controllable [1]: a so-called persistent spin helix (PSH) state [2]. For the situation of imbalanced SO interactions, geometric confinement such as nanowires also suppresses spin relaxation because orientation of the electron momentum is restricted along the wire orientation [22,30–39]. This restriction produces the unidirectional SO field for electron

*These authors contributed equally to this work.

†Corresponding author: makoto@material.tohoku.ac.jp

spin and suppresses randomization of the spin precession axis. Particularly, a nanowire with strong SO interaction provides a promising platform for realizing Majorana quasiparticles [8,9] and parafermions [40,41] towards topological quantum information processing, which requires control of the SO strength to engineer a noncollinear spin texture [42,43]. In suspended InAs nanowires, vectorial dependence of the SO interaction has been studied by anisotropic WAL in magnetoconductance with vectorial magnetic field application [44]. However, the suppressed spin relaxation comes to show WL in magnetoconductance measurements [33,34], thereby making it impossible to evaluate the SO strength by quantum correction. Recently, the relative ratio between the Rashba and linear Dresselhaus SO coefficients has been identified in narrow semiconductor wires using WL anisotropy under in-plane external magnetic fields [45,46]. For the quantification of the SO coefficients, however, some ambiguity remains because the precise extraction of the SO strength has been missed in narrow wires under the WL regime. In addition, determination of the bulk Dresselhaus SO coefficient γ in narrow gap semiconductors such as InGaAs, InAs, InSb, and others is expected to be necessary for realizing novel spin and topological states in various materials and nanostructures.

Here, we demonstrate the quantification of the full SO coefficients in III-V narrow semiconductor wires by anisotropic WL under various in-plane magnetic field orientations. We employ lithography-defined narrow wires based on an $In_{0.53}Ga_{0.47}As$/ $In_{0.52}Al_{0.48}As$ QW with a top gate electrode. By choosing the particular crystal orientation, we can quantify the ratio between Rashba (α) and linear Dresselhaus (β_1) SO coefficients. Wide-range tuning of α/β_1 solely according to the top gate enables us to distinguish predominant regions of either Rashba or Dresselhaus SO field with no fitting procedure. This makes reliable evaluation of Rashba SO coefficient possible in a separately prepared Hall bar using the WAL correction. Finally, we decompose the full SO coefficients in narrow wires including the bulk Dresselhaus SO coefficient γ, which is uniquely determined by the material. To verify the accuracy for the quantified SO strength, we compare the γ value for the Hall bar where the quantum transport is fully governed by the renormalized Dresselhaus SO interaction. The extracted γ values show good agreement between narrow wires ($\gamma = -7.0\,\mathrm{eV\,\AA^3}$) and WAL corrections ($|\gamma| = 6.8\,\mathrm{eV\,\AA^3}$). Results show that our approach can provide an important platform for full quantification of SO interactions under suppressed spin relaxation in narrow semiconductor wires. This approach therefore offers a promising route for realizing protected spin textures [1–7], exotic quasiparticles [8,9,40,41], and peculiar optical properties [11] in various materials and nanostructures and for determining fundamental band parameters in various material systems.

Using our approach, we were also able to provide a general principle to evaluate the bulk Dresselhaus coefficient γ. To evaluate the γ value in earlier studies, the potential profile in a QW was expected to be close to the PSH state [47,6] or have a negligible Rashba SO interaction [48], both of which were designed carefully by doping and application of an external gate; in some materials, there is difficulty in satisfying these conditions. Our approach, by combining the WL anisotropy in narrow wires with the WAL correction in a Hall bar, does not restrict the potential structure to close to PSH and symmetric conditions. It is applicable for various materials such as InSb-based and InAs-based nanowires.

This paper is organized as follows. In Sec. II, we explain details of the sample structure and the experimental setup of WL magnetotransport under an in-plane external magnetic field. Next, in Sec. III, we introduce the measurement principle for evaluating the relative ratio between the Rashba and linear Dresselhaus SO coefficients based on WL anisotropy. In Sec. IV, we explain the experimentally obtained results for WL in narrow wires oriented along the [−110], [010], and [110] crystal axes and evaluate the SO field orientation. In Sec. V, we show the WL anisotropy by changing the top-gate voltage to modulate the relative strength between the Rashba and linear Dresselhaus SO coefficients, which clarifies identification in the Rashba and Dresselhaus-predominant region for the carrier density. Subsequently, we emphasize the evaluation of the full SO strength using the relative ratio and complementarily measured Rashba SO interaction using WAL correction in a Hall bar in Sec. VI. We also show a quantitative comparison of the bulk Dresselhaus coefficient γ obtained from narrow wires and a Hall bar. We close the paper with the conclusion presented in Sec. VII.

II. SAMPLE STRUCTURE AND EXPERIMENTAL SETUP

We fabricate the following III-V semiconductor heterostructure, starting with the bottom layer, 200-nm *i*-$In_{0.52}Al_{0.48}As$/6-nm *n*-$In_{0.52}Al_{0.48}As$ with silicon doping $(1.2 \times 10^{18}\,\mathrm{cm^{-3}})$/6-nm *i*-$In_{0.52}Al_{0.48}As$ spacer/7-nm *i*-$In_{0.53}Ga_{0.47}As$ QW/6-nm *i*-$In_{0.52}Al_{0.48}As$ spacer/6-nm *n*-$In_{0.52}Al_{0.48}As$ with silicon doping $(3.2 \times 10^{18}\,\mathrm{cm^{-3}})$/10-nm *i*-$In_{0.52}Al_{0.48}As$ grown on a (001) InP substrate using metal-organic chemical vapor deposition. All layers are lattice-matched to the InP substrate to minimize strain-induced SO interaction. Figure 1(a) shows the calculated conduction and valence band profiles in the present 7-nm $In_{0.53}Ga_{0.47}As$/ $In_{0.52}Al_{0.48}As$ QW based on the Poisson-Schrödinger equation. Silicon doping to both sides of the $In_{0.52}Al_{0.48}As$ barrier layers induces the close to symmetric potential profile in the QW, which enables us to access both Dresselhaus and Rashba dominant regions by changing the carrier density through the top gate [Fig. 1(b)].

Effective magnetic fields along different crystal orientations for both the Rashba (α) and linear Dresselhaus (β_1) SO interactions are depicted in Fig. 1(e). The linear Dresselhaus SO strength is defined as $\beta_1 = -\gamma\langle k_Z^2\rangle$, where γ (<0) denotes the bulk Dresselhaus SO coefficient and $\langle k_Z^2\rangle$ represents the expected value of the squared wave number along the growth direction. Actually, k_Z is more or less constant over the applied gate bias voltage. We assume $\alpha < 0$, $\beta_1 > 0$, and the Landé g factor $g < 0$ based on the present potential profile in the QW. The epitaxial films are processed into 700-nm-wide wire structures of 100 μm length along [−110], [010], and [110] crystal orientations by electron-beam lithography and reactive ion etching [Fig. 1(d)]. We set 50 parallel wires in each orientation to suppress the universal conductance fluctuation, as shown in the inset microscope image in Fig. 1(d). A gate insulator of 5-nm AlO/95-nm HfO was formed by atomic layer deposition, followed by 10-nm Cr/100-nm Au top electrodes. According to the SO field symmetry in Fig. 1(e),

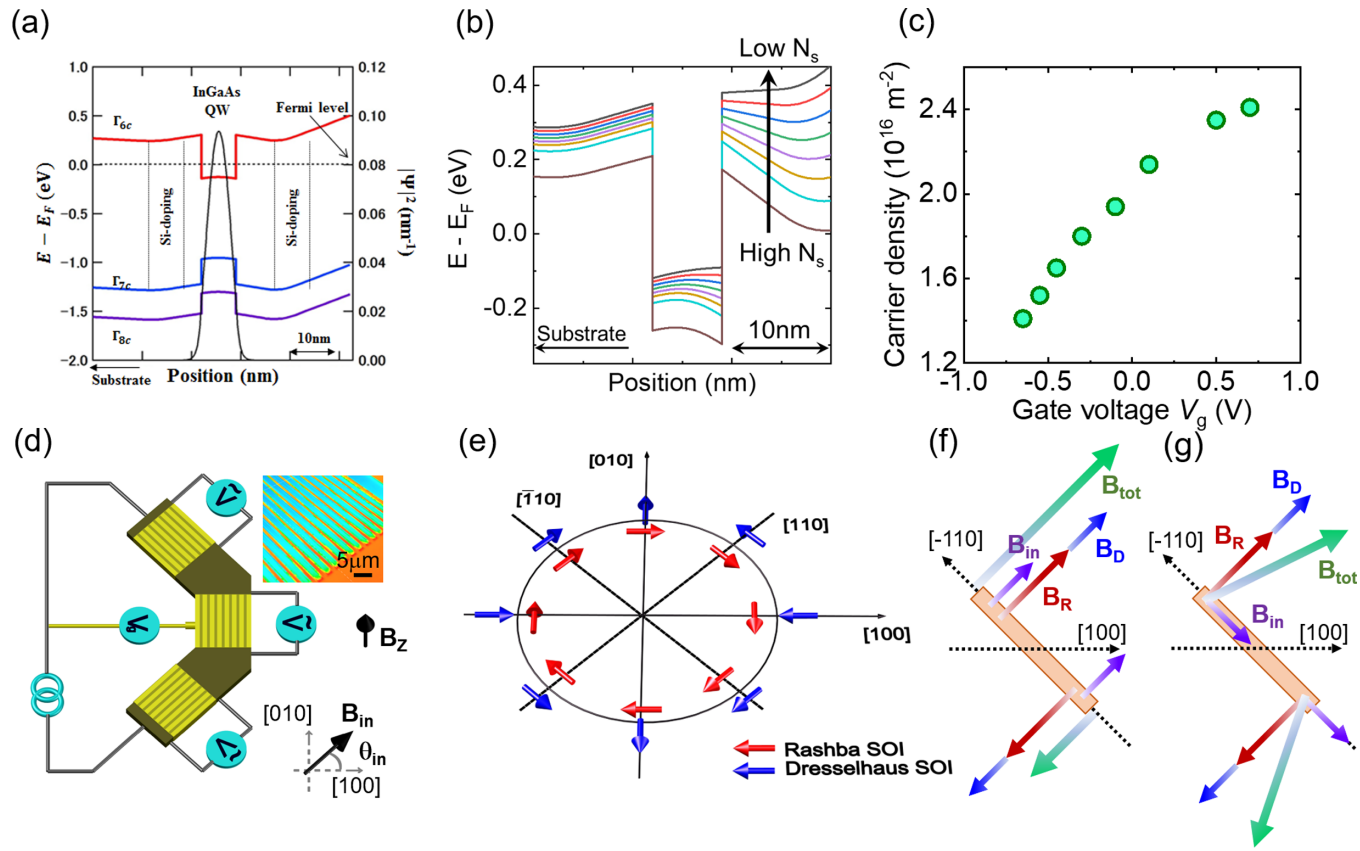

FIG. 1. (a) Conduction and valence bands as well as electron probability density in a (001) $In_{0.53}Ga_{0.47}As/In_{0.52}Al_{0.48}As$ two-dimensional electron gas calculated using the Poisson-Schrödinger equation. (b) Modulation of the conduction band profile in various sheet carrier densities modulated by the top gate. (c) Top-gate voltage dependence of sheet carrier density at $T = 1.6$ K. (d) Device configuration for parallel wire structures along [−110], [010], and [110] crystal orientations with applied perpendicular and in-plane external magnetic fields. Inset shows a microscope image for the parallel wires. (e) Schematic illustration of Rashba and Dresselhaus spin-orbit induced effective magnetic fields in the studied crystal orientations. Panels (f) and (g) show the orientations of Rashba (red), Dresselhaus (blue), and in-plane (purple) magnetic fields for [−110] wire. The in-plane field is either (f) parallel or (g) perpendicular to the spin-orbit field, inducing different configurations for the total magnetic field direction (green arrows).

the Rashba and linear Dresselhaus SO fields are mutually perpendicular in the [010] direction, whereas the two SO fields are parallel (antiparallel) in [−110] ([110]) direction. We applied a constant external magnetic field B_{in} parallel to the QW plane with angle θ_{in} defined from the [100] direction [Fig. 1(d)]. After we measured the WL using magnetoconductance in each wire by sweeping perpendicular magnetic field B_z, we continued measurements with different θ_{in}. We changed the angle of B_{in} every 2° from [100] ($\theta_{in} = 0°$) to [−100] ($\theta_{in} = 180°$) in a counterclockwise manner [Fig. 1(d)]. All measurements for wires were conducted at $T = 1.6$ K.

Figure 1(c) shows the top-gate voltage (V_g) dependence of sheet carrier density N_s for the [010] wire, changing from 1.41 to 2.41×10^{16} m^{-2} for $V_g = -0.65$ to $+0.7$ V. No second-subband occupation is observed in Shubnikov–de Haas (SdH) oscillations. Before the WL measurement, we analyzed the effective wire widths from the resistance peaks before starting SdH oscillations in each wire [49]. Because of carrier depletion from the sidewall, the effective wire width W_{eff} is reduced to 320–396 nm, which is consistent with the value reported from an earlier study [34]. To analyze the Rashba or Dresselhaus SO strengths separately from the wire based on WAL corrections to conductivity, Hall bar structures with 20 μm width and 160 μm length are processed and magnetotransport measurements are conducted at $T = 0.3$ K.

III. PRINCIPLE FOR DETECTING SPIN-ORBIT FIELDS BY WEAK LOCALIZATION ANISOTROPY

To quantify the relative ratio between the Rashba and linear Dresselhaus SO strengths in narrow wires with no fitting by quantum correction theory, we use the modulation of the WL amplitude caused by spin relaxation anisotropy under different angles of in-plane external magnetic fields [46]. This modulation enables us to evaluate the SO field orientation by using the following physics [45]. We consider a one-dimensional (1D) quantum wire oriented along the [−110] axis in Figs. 1(f) and 1(g). For simplicity of the argument, we assume purely 1D wire because the orientation of the electron momentum is well defined. We can extend the argument for a finite wire width W smaller than the spin precession length $L_{so} = \pi\hbar^2/m^*(\alpha + \beta)$, where $\hbar$ is the reduced Planck's constant and where m^* represents an electron's effective mass, because spin relaxation is suppressed for $W \ll L_{so}$ [45].

Because of the lateral confinement of electron momentum along the wire direction, for a [−110] wire, the Rashba and Dresselhaus SO fields are oriented perpendicular to the wire direction and mutually parallel [red (Rashba) and blue (Dresselhaus) arrows in Figs. 1(f) and 1(g)]. Whereas D'yakonov-Perel' (DP) spin relaxation [14] results from randomization of the spin precession axis, spin is now a conserved quantity in a 1D wire due to the unidirectional spin precession axis, suppressing spin relaxation [30–39]. The SO field is opposite for electrons moving along the [−110] and [1–10] directions, resulting in no phase accumulation for electron waves in symmetric paths. When the in-plane external field $B_{\rm in}$ is applied parallel to this SO field [purple arrows in Fig. 1(f)], the total magnetic field remains unidirectional [green arrows in Fig. 1(f)], thereby preserving the suppressed DP spin relaxation. However, when $B_{\rm in}$ is not parallel to the SO field [purple arrows in Fig. 1(g)], the total magnetic field is no longer unidirectional [green arrows in Fig. 1(g)], causing DP spin relaxation through randomization of the spin precession axis. This relaxation leads to additional dephasing for electrons in a time-reversal symmetric path and engenders reduction of the WL amplitude [45,46]. Since the direction of the spin precession axis fluctuates the most when the applied in-plane magnetic field is equal to the SO field, WL anisotropy from rotating the in-plane field is most pronounced when magnitudes of the in-plane field and SO effective field are close to each other.

The conductance correction ΔG from diagrammatic perturbation theory [15] is proportional to $C_{00} - \sum_{m=-1}^{1} C_{1m}$, where C_{00} and C_{1m} represent the singlet and triplet terms to the conductance, respectively. The singlet term contributes to positive conductance, which is unaffected by DP spin relaxation, but is suppressed under an in-plane magnetic field. The triplet term gives a negative conductance contribution, and is suppressed by the enhancement of spin relaxation. It is noteworthy that the singlet term contributing to positive conductance is now suppressed by an in-plane magnetic field. When the in-plane magnetic field is applied nonparallel to the SO field orientation, the triplet term is reduced because of the enhanced spin relaxation, leading to a reduced amplitude of the negative conductance correction. However, when the in-plane magnetic field is aligned along the SO field, spin is still a good quantum number that exerts no influence on the triplet term. This lack of influence preserves the negative conductance correction. Such conductance modulation against the in-plane field angle is reflected in the WL amplitude: the maximum WL amplitude corresponds to the parallel configuration between the in-plane magnetic field and SO effective field. By applying this physical principle to the [010] wire, where the Rashba and Dresselhaus SO fields are mutually perpendicular, as shown below in greater detail, we can identify the relative ratio between α and β_1 by measuring the WL at different $B_{\rm in}$ angles.

IV. WEAK LOCALIZATION IN [−110]-, [010]-, AND [110]-ORIENTED WIRES UNDER VARIOUS IN-PLANE EXTERNAL MAGNETIC FIELD ANGLES

We first measure magnetoconductance under various in-plane field angles $\theta_{\rm in}$ at $B_{\rm in} = 1.5$ T and $V_{\rm g} = -0.15$ V. In the following experiments in Secs. IV and V, the SO effective field is ranging between 2.5 to 6.5 T depending on the gate voltage. We set the magnitude of in-plane field $B_{\rm in}$ between 1.5 and 2.0 T, corresponding to a ratio between $B_{\rm in}$ and SO fields of around 0.3 to 1.0. Figures 2(a)–2(c) show the color-coded magnetoconductance as a function of perpendicular field $B_{\rm z}$ and in-plane field angle $\theta_{\rm in}$ in [−110]-, [010]-, and [110]-oriented wires. $B_{\rm in}$ is rotated from [100] ($\theta_{\rm in} = 0^\circ$) to [−100] ($\theta_{\rm in} = 180^\circ$) through the [010] ($\theta_{\rm in} = 90^\circ$) axis. In all wires, the conductance amplitude defined by $\Delta\sigma$ increases with the increase of $B_{\rm z}$, shown as the color-code change from blue (minimum) to red (maximum) in Figs. 2(a)–2(c), being a clear indication of the WL signal and suppressed spin relaxation through lateral confinement [45,46]. In addition, the amplitude of the WL is a anisotropic with respect to the in-plane field angle $\theta_{\rm in}$, as presented in Fig. 2(g) for the [010] wire, where the maximum WL is achieved at $\theta_{\rm in} = 35^\circ$, and the minimum appears at $\theta_{\rm in} = 125^\circ$. It should be also noted that the widths of the WL curves at $\theta_{\rm in} = 35^\circ$ and 125° are identical, indicating the negligible modulation of the WL width from the in-plane $B_{\rm in}$ field. As indicated by the dashed lines in Figs. 2(a)–2(c), the $\theta_{\rm in}$ giving the maximum WL amplitude depends on the wire directions, corresponding to $\theta_{\rm in} = 45^\circ$, 35°, and 135° for [−110], [010], and [110] wires, respectively. The maximum WL amplitude corresponds to the most suppressed spin relaxation against the in-plane magnetic field angle. In Figs. 2(d)–2(f), the sums of Rashba and Dresselhaus SO field vectors in [−110], [010], and [110] wires are depicted, respectively, as pink, light green, and light blue arrows. Depending on the wire orientations with respect to the crystal axis, the total SO field from the Rashba and Dresselhaus SO interaction changes both strength and direction. Whereas the total SO field for the [−110] and [110] wires are perpendicular to the wire orientation (either 45° or 135° with respect to [100] axis [Figs. 2(d) and 2(f)]), the SO field orientation depends on the relative strength between the Rashba and Dresselhaus SO interactions for the [010] wire [Fig. 2(e)]. The angles of maximum WL amplitude observed experimentally in Figs. 2(a)–2(c) correspond to these total SO field directions.

To extract the SO field angle $\theta_{\rm eff}$ precisely, we plot the in-plane magnetic field angle $\theta_{\rm in}$ dependence of the WL amplitude $\Delta\sigma$ at fixed $B_{\rm z}$ (=20 mT) in each wire, an example of which is presented in Fig. 2(h) for the [010] wire. Because of the spatial symmetry of the measurement configuration [46], we safely extend the result to $180^\circ \leqslant \theta_{\rm in} \leqslant 360^\circ$. The data and extrapolation of $\Delta\sigma(B_{\rm z} = 20\ {\rm mT})$ together show oscillatory behavior with respect to the in-plane field angle $\theta_{\rm in}$, indicating that electron coherence caused by WL is modulated by anisotropic spin relaxation, as discussed in Sec. III. We also extend the result to $180^\circ \leqslant \theta_{\rm in} \leqslant 360^\circ$ for the polar figures in Figs. 2(i) and 3(a). By defining the normalized conductance modulation as $\Delta\tilde{\sigma} = [\Delta\sigma(B_{\rm z} = 20\ {\rm mT}) - \Delta\sigma_{\rm min}]/(\Delta\sigma_{\rm max} - \Delta\sigma_{\rm min})$, where $\Delta\sigma_{\rm min}$ ($\Delta\sigma_{\rm max}$) corresponds to the minimum (maximum) conductance value under the in-plane field angle $\theta_{\rm in}$ dependence [grey dashed lines in Fig. 2(h)], we plot the polar figure of $\Delta\tilde{\sigma}$ for the [−110], [010], and [110] wires respectively as red, green, and blue circles in Fig. 2(i). For the [−110] and [110] wires, $\Delta\tilde{\sigma}$ peaks at a $\theta_{\rm in}$ of 45° and 135°, respectively, because both the Rashba and linear Dresselhaus SO fields are perpendicular to

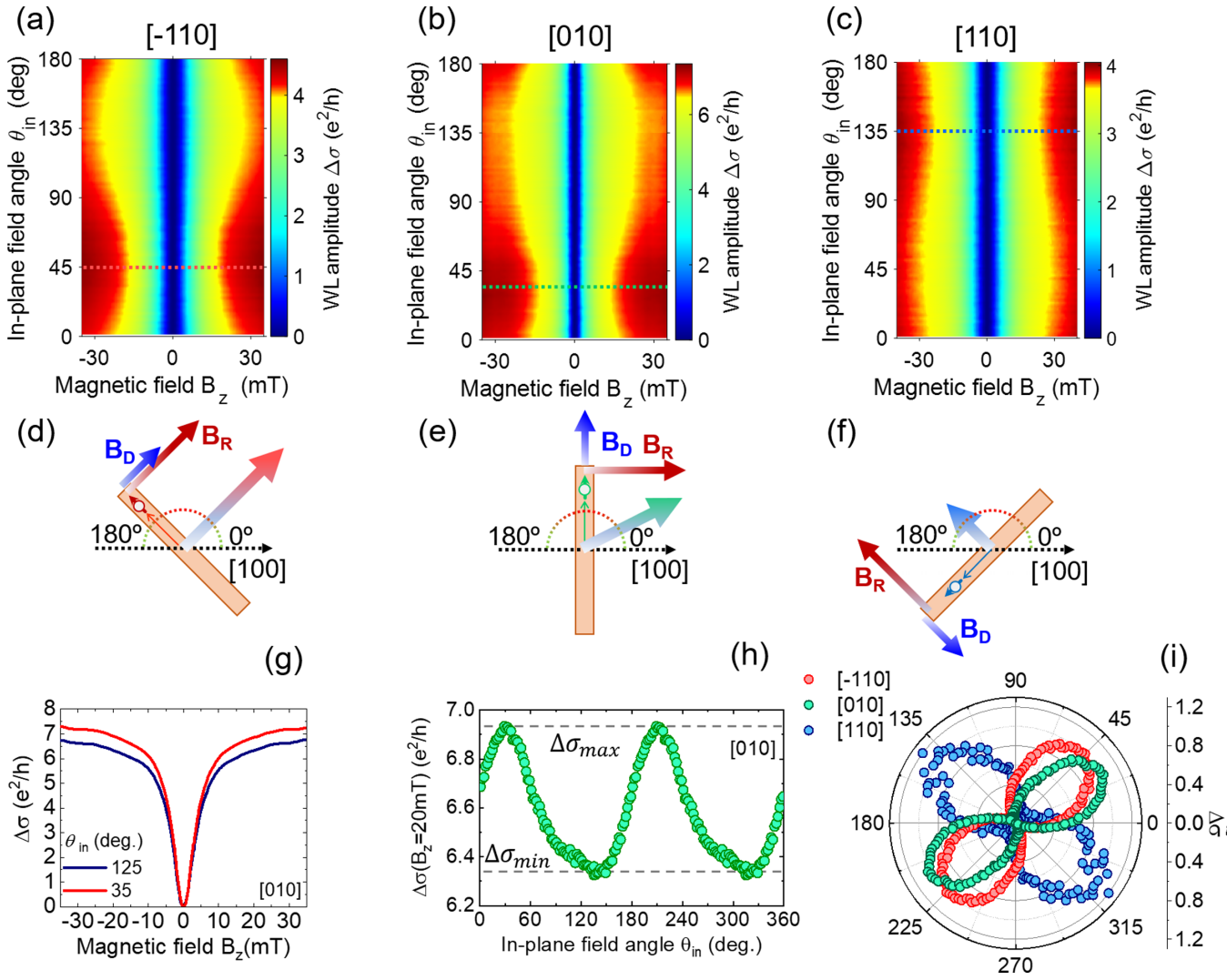

FIG. 2. Color-coded magnetoconductance as functions of perpendicular magnetic field B_z and in-plane magnetic field angle θ_{in} for (a) [−110], (b) [010], and (c) [110] wires at $B_{\text{in}} = 1.5$ T. (d)–(f) Schematic illustration of Rashba (red), Dresselhaus (blue), and total spin–orbit fields (pink, light green, and light blue arrows) for (d) [−110], (e) [010], and (f) [110] wires. (g) Magnetoconductance of [010] wire with maximum (red) and minimum (blue) weak localization amplitude, respectively, at $\theta_{\text{in}} = 35°$ and 125°. (h) Conductance amplitude $\Delta\sigma$ at fixed $B_z = 20$ mT as a function of θ_{in} for [010] wire. Dashed lines correspond to the maximum and minimum conductance amplitude $\Delta\sigma_{\text{max}}$ and $\Delta\sigma_{\text{min}}$. (i) Polar plot of normalized conductance $\Delta\tilde{\sigma}$ as a function of in-plane field angle for [−110] (red), [010] (green), and [110] (blue) wires.

the wire direction [Figs. 2(d) and 2(f)]. The θ_{eff} obtained in the experiment shows perfect agreement with the expected SO field angle, confirming the precise evaluation of the SO field direction. Additionally, we can directly obtain the ratio between α and β_1 from the [010] wire by taking advantage of the perpendicular orientation between Rashba and linear Dresselhaus SO fields [Fig. 2(e)]. We note that the cubic Dresselhaus SO interaction becomes zero in the [010] crystal orientation. In the [010] wire, the relation between α/β_1 and θ_{eff} is described simply as [45],

$$\frac{\alpha}{\beta_1} = -\cot\theta_{\text{eff}}. \tag{1}$$

In Fig. 2(i), the [010] wire exhibits θ_{eff} at 35°, from which we can ascertain $\alpha/\beta_1 = -1.43$ directly. One can use Eq. (1) to evaluate arbitrary α/β_1 ratio in wire structures based on the anisotropic WL observed in magnetoconductance measurements.

V. GATE CONTROL OF THE MAXIMUM WEAK LOCALIZATION ANGLE

In order to tune the α/β_1 ratio over a wide range to expose the predominant region of Rashba or Dresselhaus SO interaction, we modulate the Rashba SO coefficient using a top gate [50] and extend the anisotropic WL measurement in the [010] wire for different V_g at $B_{\text{in}} = 2.0$ T. Figure 3(a) shows polar plots of $\Delta\tilde{\sigma}$ for $V_g = -0.55$, -0.45, and $+0.10$ V. With decreasing V_g, i.e., lowering carrier density, θ_{eff} rotates from 25° ($\alpha/\beta_1 = -2.14$) to 65° ($\alpha/\beta_1 = -0.47$) through 45° ($\alpha/\beta_1 = -1$), i.e., the PSH state. Decrease of the α/β_1 ratio corresponds to the reduction of Rashba SO coefficient with decreasing N_s.

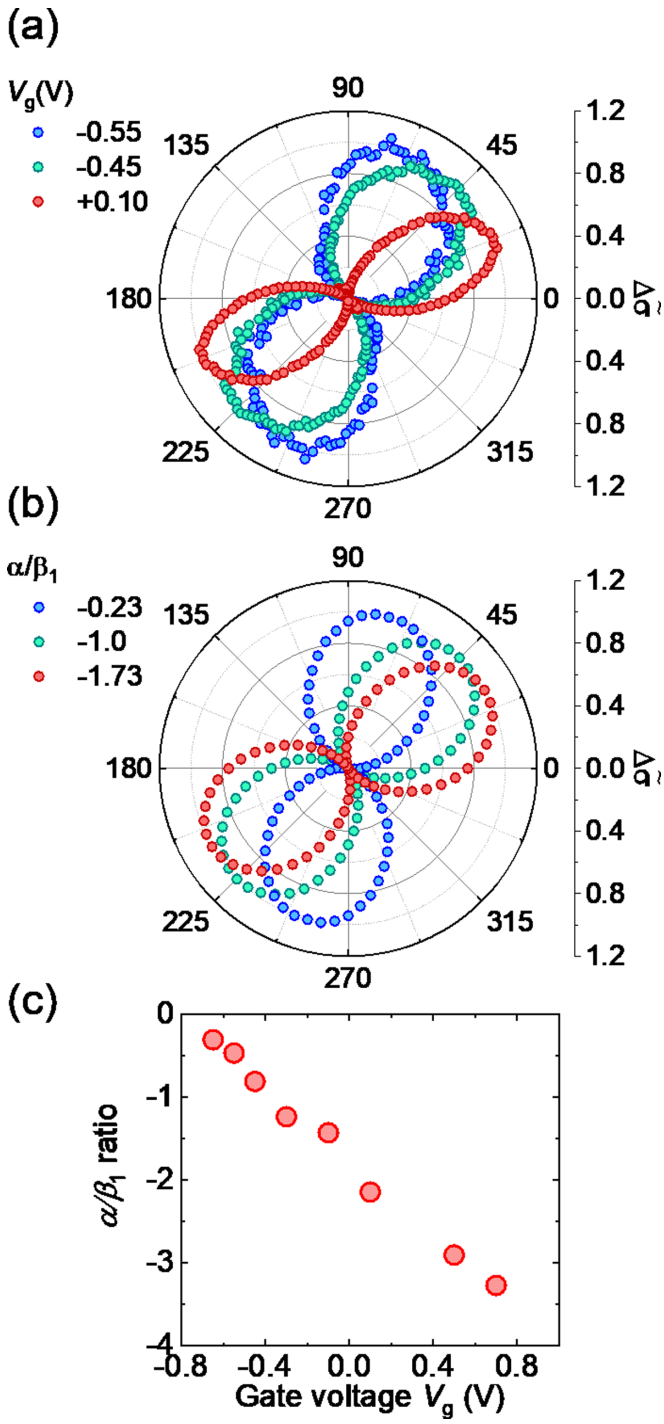

FIG. 3. (a) Polar plot of normalized conductance $\Delta\tilde{\sigma}$ as a function of in-plane field angle under different top-gate voltage: $V_g = -0.55$, -0.45, and $+0.10$ V under $B_{\rm in} = 2.0$ T. (b) Polar plot of numerically computed conductance for different α/β_1 ratio: $\alpha/\beta_1 = -0.23$, -1, and -1.73. (c) Gate voltage dependence of α/β_1 ratio for [010] wire under $B_{\rm in} = 2.0$ T.

Figure 1(b) shows the calculated potential profiles in the conduction band by changing the sheet carrier density N_s from high N_s (2.0×10^{16} m^{-2}) to low N_s (0.44×10^{16} m^{-2}) using the top gate. With the lowering of the sheet carrier density, the potential structure inside of the $In_{0.53}Ga_{0.47}As$ QW becomes more symmetric. Further reduction of the sheet carrier density changes the sign of the potential gradient. Such modulation of the conduction band profile corresponds to a reduction of the Rashba SO coefficient α and the crossing $\alpha = 0$. In this experiment, the ratio of α/β_1 decreases upon lowering of the carrier density, which is consistent with the calculated potential profile modulation by the gate, i.e., reduction of the Rashba SO coefficient.

To confirm the variation of the WL anisotropy with V_g further, we computed the WL under a $B_{\rm in}$ using magnetotransport of disordered wire conductors numerically under different α/β_1 ratios. The calculations are based on an efficient recursive Green's function algorithm within the Landauer-Büttiker formalism [51–53], since we have confirmed this Green's function approach described the physics of WL anisotropy [45] under a $B_{\rm in}$ and captured the experimentally observed variation of WL anisotropy [46]. Because of the limited energy scales smaller than the realistic Fermi energies, we chose the parameters for wire width, length, disorder potential, Fermi energy, and number of disorders respectively as $W = 240$ nm, $L = 800$ nm, $\bar{U}_{\rm dis} = U_{\rm dis}/t_0 = 1.4$, $\bar{E}_F = E_F/t_0 = 0.5$, and $N_d = 1200$, which satisfy the quasi-1D transport observed in the experiment. Here, t_0 is an energy unit defined by $\hbar^2/(2m^*a^2)$, where a is the lattice constant. The disorder potential is modeled using Anderson disorder with a strength $\bar{U}_{\rm dis}$. Wire conductance is obtained by averaging over N_d disorder configurations. It is analyzed using normalized conductance modulation. Figure 3(b) shows the numerically computed $\Delta\tilde{\sigma}$ for $\alpha/\beta_1 = -0.23$, -1, and -1.73, which perfectly reproduces the expected $\theta_{\rm eff} = 77°$, $45°$, and $30°$, respectively, from Eq. (1), and the rotation towards 90° by reducing the α/β_1 ratio in the experiment. We also reproduced a similar dependence of the WL anisotropy by employing universal modeling of quantum interference effects based on real-space simulation [27], the details of which will be discussed in Sec. VI and the Supplemental Material [49]. Through the top gate dependence of the in-plane field angle at the maximum WL amplitude, the potential profile from the carrier modulation, and by the simulated WL anisotropy, we demonstrate modulation of the SO field direction using the top gate. Quantification of the α/β_1 value from the [010] wire is advantageous to evaluate the arbitrary ratios of α/β_1, independent of the quantum correction model and with no fitting procedures.

In Fig. 3(c), a plot shows the experimentally evaluated α/β_1 between $V_g = -0.65$ ($N_s = 1.41 \times 10^{16}$ m^{-2}) and $+0.7$ V ($N_s = 2.41 \times 10^{16}$ m^{-2}) in the [010] wire. The value of α/β_1 is widely modulated from Dresselhaus-predominant ($\alpha/\beta_1 = -0.31$) to Rashba-predominant ($\alpha/\beta_1 = -3.27$) solely by the gate. Quantifying the α/β_1 ratio to identify the dominated SO interaction becomes crucially important to choose the appropriate quantum correction theory because the developed models rely on the specific condition of the SO interactions, either Rashba or Dresselhaus or the full SO coefficients [16–29]. The Rashba dominant region in the carrier density $N_s > 2.4 \times 10^{16}$ m^{-2} can be identified which supports reliable evaluation of α values from WAL analysis in a Hall bar by application of two-dimensional quantum correction theory [21].

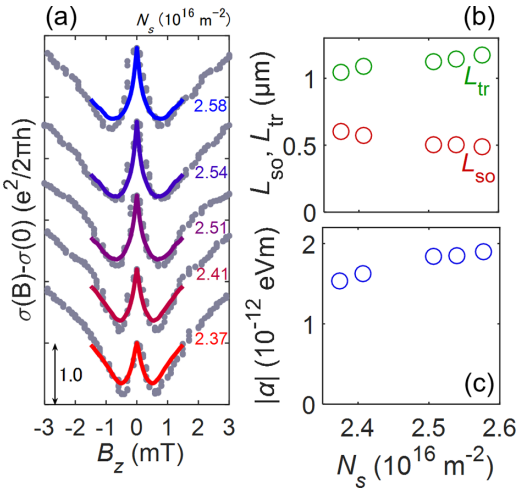

FIG. 4. (a) Magnetoconductance measured in a Hall bar at $T = 0.3$ K in a Rashba-predominant region by setting the sheet carrier density N_s between 2.37×10^{16} and 2.58×10^{16} m^{-2}. Solid colored lines correspond to fits using universal modeling of WAL corrections based on the real-space simulation developed by Sawada *et al.* [27]. (b) Extracted spin-orbit length L_{SO} and mean free path L_{tr} as a function of carrier density. The $L_{tr} > L_{SO}$ corresponds to the ballistic regime for WAL corrections. (c) Rashba spin-orbit coefficient $|\alpha|$ as a function of carrier density.

VI. EVALUATION OF FULL SPIN-ORBIT COEFFICIENTS IN WIRES

Evaluation of an arbitrary ratio between the Rashba and linear Dresselhaus SO coefficients, and the wide range control of the α/β_1 value by the top gate, enable us to identify the full SO coefficients in narrow wires by complementarily using the WAL correction in a Hall bar. First, to evaluate the Rashba SO coefficient, we measured the magnetoconductance in a Hall bar device at $T = 0.3$ K. Based on the consideration of α/β_1 as evaluated from the [010] wire, the Rashba SO interaction becomes the dominant contribution to the magnetoconductance by setting the sheet carrier density N_s between 2.37×10^{16} m^{-2} and 2.58×10^{16} m^{-2}. Figure 4(a) presents the magnetoconductance found for different N_s, all of which exhibit WAL near zero magnetic fields. The conductance minimum in WAL is shifted to higher magnetic fields as the sheet carrier density increases, indicating an increase of the Rashba SO coefficient. Evaluating the Rashba SO parameter $|\alpha|$ quantitatively demands identification of the proper quantum correction theory. The mean free path L_{tr}, defined by $v_F \tau_{tr}$, where v_F is the Fermi velocity and τ_{tr} is the electron's momentum scattering time, is found to be longer than SO length $L_{SO} = \hbar^2/2m^*|\alpha|$, corresponding to the ballistic regime. Because the quantum correction based on the Iordanskii, Lyanda-Geller, and Pikus (ILP) theory is only valid in the diffusive regime, which should satisfy the condition of $L_{SO} > L_{tr}$ [16], we employ universal modeling of WAL corrections based on real-space simulation developed by Sawada *et al.* [27]. In this simulation, SO interactions are included as one-electron interaction propagators associated with closed scattering loops of electrons, which are generated using a pseudorandom-number generator. Because a Boltzmannian picture of electrons is assumed, the salient advantage of this model is that (1) both diffusive and ballistic regions are available for the WAL correction to magnetoconductance and (2) full SO coefficients are considered [49]. It is also noteworthy that this approach is equivalent to the Golub model, which can also treat both ballistic and diffusive regimes and can also be useful for a high mobility QW [20,23,25]. Because the Sawada model is specialized for modeling the quantum correction of conductivity, the time required for a simulation of WAL is reasonably fast in comparison with the Green's function approach [45], which is useful for data fitting. In addition, we have confirmed that our simulation based on the Sawada model reproduces an earlier report of literature [Fig. 2(b) in Ref. [20]], indicating the validity of our simulation for application to experimentally obtained results. Solid colored lines in Fig. 4(a) show fitting results based on the Sawada model by solely considering the Rashba SO coefficient, where the model reproduces the observed WAL well. Then we extract the SO length L_{SO} and Rashba SO coefficient $|\alpha|$ as functions of N_s, shown respectively in Figs. 4(b) and 4(c). We find that the mean free path L_{tr} is much longer than L_{SO} and the evaluated $|\alpha|$ decreases monotonically with lowering N_s.

Figure 5(a) presents a summary of the evaluated $|\alpha|$ (open blue squares) and α/β_1 ratio (open red circles) as a function of N_s. The linear dependence of $|\alpha|$ to the carrier density reflects the linear scaling of internal electric field inside the InGaAs QW, enabling us to extend the variation of $|\alpha|$ in the lower N_s region [dashed blue line in Fig. 5(a)]. Comparison with the α/β_1 ratio [open red circles in Fig. 5(a)] shows that the carrier densities for a vanishing Rashba SO interaction, i.e., $|\alpha| = 0$ and $\alpha/\beta_1 = 0$, become mutually equal. This finding confirms unambiguously (1) that the WAL correction in magnetoconductance is dominated by the Rashba SO interaction and (2) that the separation of the Rashba-predominant region from the α/β_1 ratio in the wire is the correct approach to identify a suitable model for the quantum correction of the conductivity. Based on the α/β_1 ratio together with the extracted Rashba SO coefficient $|\alpha|$ in Fig. 5(a), the unknown parameter in Eq. (1) becomes the bulk Dresselhaus coefficient γ because $\langle k_Z^2 \rangle$ is obtained numerically based on $\langle k_Z^2 \rangle = \int_0^\infty \Psi(z)\partial^2/\partial z^2 \Psi(z) dz$, where $\Psi(z)$ is the electron wave function in a QW calculated using the Poisson-Schrödinger equation [49]. Then we can ascertain the γ value, i.e., the full SO coefficient in the wires. Figure 5(b) shows θ_{eff} as a function of N_s. The solid line corresponds to the fit using Eq. (1). A rapid increase of θ_{eff} with the reduction of the carrier density reproduces with $\gamma = -7.0$ eV Å^3, resulting in the electrical determination of the bulk Dresselhaus coefficient in narrow wires. Now the Rashba and Dresselhaus SO parameters are fully decoupled from the α/β_1 ratio in the wire and are shown as $|\alpha|$, $|\beta_1|$, and $|\beta_3|$ in Fig. 5(a).

To confirm the validity of the SO coefficients obtained by anisotropic WL measurements in the [010] wire together with the WAL correction to the conductivity in the Hall bar, we compare the bulk Dresselhaus coefficient γ using a gate-fitted Hall bar. To evaluate the Dresselhaus SO coefficient, we tuned the carrier density to be $N_s = 1.38 \times 10^{16}$ m^{-2} which corresponds to the $|\alpha| = 0$ and $\alpha/\beta_1 = 0$ condition in Fig. 5(a) and measured the WAL, where the Dresselhaus SO coefficient becomes dominant because of the symmetric

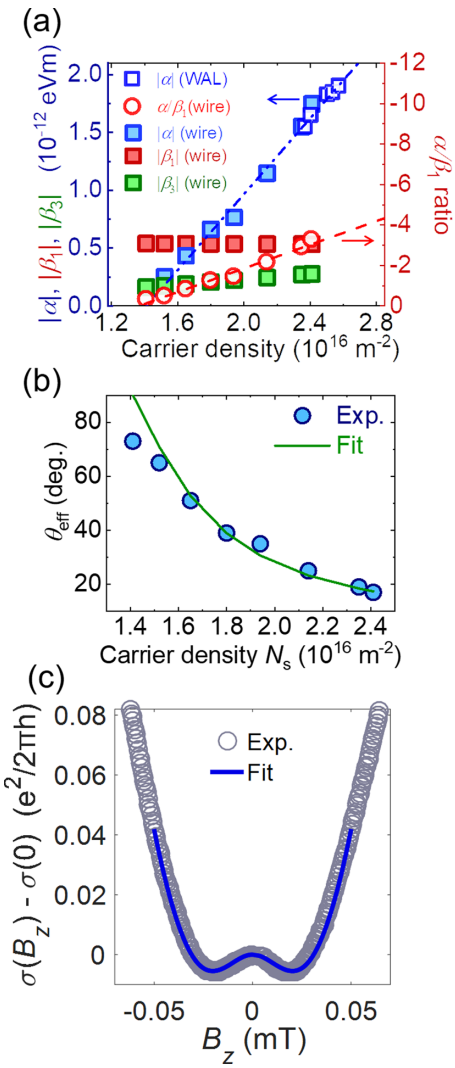

FIG. 5. (a) Carrier density dependence of Rashba $|\alpha|$ parameters (open blue squares) in a Hall bar and α/β_1 ratio (open red circles) obtained from [010] wire. Full spin-orbit coefficients $|\alpha|$, $|\beta_1|$, and $|\beta_3|$, in wires are shown as blue, red, and green squares. (b) Carrier density dependence of spin-orbit induced effective field angle $\theta_{\rm eff}$ for [010] wire and fit (solid green line) using Eq. (1). (c) Magnetoconductance originating from the Dresselhaus spin-orbit interaction in a Hall bar at $T = 0.3$ K. The carrier density at which the Rashba SO coefficient is vanished $N_s = 1.38 \times 10^{16}$ m^{-2}. The solid blue line corresponds to fitting using the Sawada model.

potential in the QW [16]. The fit by the Sawada model is presented in Fig. 5(c). Here, we only considered the linear (β_1) and cubic (β_3) Dresselhaus SO interactions for fitting, as shown in the solid blue lines in Fig. 5(c). We evaluated $\beta_1 = 5.03 \times 10^{-13}$ eV m and $\beta_3 = 1.47 \times 10^{-13}$ eV m. Based on these values, we can obtain the bulk Dresselhaus coefficient $|\gamma| = 6.8$ eV Å^3 with $\langle k_Z^2 \rangle = 0.074$ nm^{-2}, which agrees well for $\gamma = -7.0$ eV Å^3 from the [010] wire. We infer from these quantitative comparisons that our approach for quantifying the full SO coefficients in narrow wires is promising to evaluate the SO strength, even with suppressed spin relaxation, i.e., the WL region.

VII. CONCLUSION

In conclusion, we have experimentally demonstrated the quantification of the full spin-orbit coefficients in semiconductor nanowires based on a (001) $In_{0.53}Ga_{0.47}As/In_{0.52}Al_{0.48}As$ two-dimensional electron gas. We measured magnetoconductance under various angles of in-plane external magnetic fields. Magnetoconductance exhibits weak localization as a result of the suppressed spin relaxation because the electron momentum orientation is confined along the wire direction. By applying a constant in-plane magnetic field, the observed weak localization is modulated further in its amplitude depending on the relative angle between spin-orbit and in-plane magnetic fields. It reaches a maximum value when the in-plane field is parallel to the spin-orbit field. By taking advantage of the perpendicular orientation between Rashba and Dresselhaus spin-orbit fields in the [010]-oriented wires, the ratio between the Rashba and linear Dresselhaus spin-orbit coefficients α/β_1 was evaluated using no fitting procedures. Furthermore, by tuning the Rashba spin-orbit interaction using a top gate, we modulate the α/β_1 ratio from -0.31 to -3.27, from Dresselhaus-predominant to Rashba-predominant regions, using only the gate. Together with weak antilocalization in a Hall bar dominated by the Rashba spin-orbit interaction in the top gate, we quantify the full spin-orbit coefficients in the wire, including the bulk Dresselhaus coefficient of $\gamma = -7.0$ eV Å^3. The obtained γ shows good agreement with $|\gamma| = 6.8$ eV Å^3 evaluated separately from the weak antilocalization under the Dresselhaus spin-orbit interaction, confirming the precise determination of the bulk Dresselhaus coefficient in narrow wires by electrical means. As narrow wires with strong spin-orbit interaction become a platform for Majorana particles and parafermions for topological electronics as well as quantum computation, our approach will be able to provide a method to quantify the spin-orbit strength in semiconductor wires. It is applicable not only for zinc-blende structures but also for other crystals such as wurtzite, perovskite, and honeycomb structures holding the spin-orbit field in the plane, presenting potential for determining γ in widely diverse materials.

ACKNOWLEDGMENTS

We thank Prof. S. Karube and Dr. R. Thompson for fruitful discussion. We acknowledge financial support from the Japanese Ministry of Education, Culture, Sports, Science, and Technology (MEXT) Grant-in-Aid for Scientific Research (Grants No. 15H02099, No. 15H05854, No. 25220604, and No. 15H05699), EPSRC-JSPS Core-to-Core program (Grant No. JPJSCCA20160005), and the Cooperative Research Project Program of the Research Institute of Electrical Communication, Tohoku University.

[1] J. Schliemann, J. C. Egues, and D. Loss, Nonballistic Spin-Field-Effect Transistor, Phys. Rev. Lett. **90**, 146801 (2003).

[2] B. A. Bernevig, J. Orenstein, and S-C. Zhang, Exact SU(2) Symmetry and Persistent Spin Helix in a

Spin-Orbit Coupled System, Phys. Rev. Lett. **97**, 236601 (2006).

[3] J. D. Koralek, C. P. Weber, J. Orenstein, B. A. Bernevig, S.-C. Zhang, S. Mack, and D. D. Awschalom, Emergence of the persistent spin helix in semiconductor quantum wells, Nature (London) **458**, 610 (2009).

[4] M. P. Walser, C. Reichl, W. Wegscheider, and G. Salis, Direct mapping of the formation of a persistent spin helix, Nat. Phys. **8**, 757 (2012).

[5] M. Kohda, V. Lechner, Y. Kunihashi, T. Dollinger, P. Olbrich, C. Schönhuber, I. Caspers, V. V. Bel'kov, L. E. Golub, D. Weiss, K. Richter, J. Nitta, and S. D. Ganichev, Gate-controlled persistent spin helix state in (In,Ga)As quantum wells, Phys. Rev. B **86**, 081306(R) (2012).

[6] F. Dettwiler, J. Fu, S. Mack, P. J. Weigele, J. C. Egues, D. D. Awschalom, and D. M. Zumbühl, Stretchable Persistent Spin Helices in GaAs Quantum Wells, Phys. Rev. X **7**, 031010 (2017).

[7] J. Fu, P. H. Penteado, M. O. Hachiya, D. Loss, and J. C. Egues, Persistent Skyrmion Lattice of Noninteracting Electrons with Spin-Orbit Coupling, Phys. Rev. Lett. **117**, 226401 (2016).

[8] Y. Oreg, G. Refael, and F. von Oppen, Helical Liquids and Majorana Bound States in Quantum Wires, Phys. Rev. Lett. **105**, 177002 (2010).

[9] R. M. Lutchyn, J. D. Sau, and S. Das Sarma, Majorana Fermions and a Topological Phase Transition in Semiconductor-Superconductor Heterostructures, Phys. Rev. Lett. **105**, 077001 (2010).

[10] Xiao-Liang Qi and Shou-Cheng Zhang, Topological insulators and superconductors, Rev. Mod. Phys. **83**, 1057 (2011).

[11] Z. Li, F. Marsiglio, and J. P. Carbotte, Vanishing of interband light absorption in a persistent spin helix state, Sci. Rep. **3**, 2828 (2013).

[12] E. I. Rashba, Properties of semiconductors with an extremum loop. I. Cyclotron and combinational Resonance in a magnetic field perpendicular to the plane of the loop, Sov. Phys. Solid State **2**, 1109 (1960)]; Y. A. Bychkov and E. I. Rashba, Oscillatory effects and the magnetic susceptibility of carriers in inversion layers, J. Phys. C: Solid State Phys. **17**, 6039 (1984).

[13] G. Dresselhaus, Spin-orbit coupling effects in zinc blende structures, Phys. Rev. **100**, 580 (1955).

[14] M. I D'yakonov and V. I. Perel', Spin orientation of electrons associated with the interband absorption of light in semiconductors, JETP **33**, 1053 (1971).

[15] S. Hikami, A. I. Larkin, and Y. Nagaoka, Spin-orbit interaction and magnetoresistance in the two dimensional random system, Prog. Theor. Phys. **63**, 707 (1980).

[16] S. V. Iordanskii, Y. B. Lyanda-Geller, and G. E. Pikus, Weak localization in quantum wells with spin-orbit interaction, JETP Lett. **60**, 206 (1994).

[17] F. G. Pikus and G. E. Pikus, Conduction-band spin splitting and negative magnetoresistance in A_3B_5 heterostructures, Phys. Rev. B **51**, 16928 (1995).

[18] W. Knap, C. Skierbiszewski, A. Zduniak, E. Litwin-Staszewska, D. Bertho, F. Kobbi, J. L. Robert, G. E. Pikus, F. G. Pikus, S. V. Iordanskii *et al.*, Weak antilocalization and spin precession in quantum wells, Phys. Rev. B **53**, 3912 (1996).

[19] J. B. Miller, D. M. Zumbühl, C. M. Marcus, Y. B. Lyanda-Geller, D. Goldhaber-Gordon, K. Campman, and A. C. Gossard, Gate-Controlled Spin-Orbit Quantum Interference Effects in Lateral Transport, Phys. Rev. Lett. **90**, 076807 (2003).

[20] L. E. Golub, Weak antilocalization in high-mobility two-dimensional systems, Phys. Rev. B **71**, 235310 (2005).

[21] A. Punnoose, Magnetoconductivity in the presence of Bychkov–Rashba spin–orbit interaction, Appl. Phys. Lett. **88**, 252113 (2006).

[22] S. Kettemann, Dimensional Control of Antilocalization and Spin Relaxation in Quantum Wires, Phys. Rev. Lett. **98**, 176808 (2007).

[23] M. M. Glazov and L. E. Golub, Nondiffusive weak localization in two-dimensional systems with spin–orbit splitting of the spectrum, Semiconductors **40**, 1209 (2006).

[24] M. Kammermeier, P. Wenk, J. Schliemann, S. Heedt, T. Gerster, and Th. Schäpers, Magnetoconductance correction in zinc-blende semiconductor nanowires with spin–orbit coupling, Phys. Rev. B **96**, 235302 (2017).

[25] M. M. Glazov and L. E. Golub, Spin–orbit interaction and weak localization in heterostructures, Semicond. Sci. Technol. **24**, 064007 (2009).

[26] M. Kammermeier, P. Wenk, and J. Schliemann, Control of Spin Helix Symmetry in Semiconductor Quantum Wells by Crystal Orientation, Phys. Rev. Lett. **117**, 236801 (2016).

[27] A. Sawada and T. Koga, Universal modeling of weak antilocalization corrections in quasi-two-dimensional electron systems using predetermined return orbitals, Phys. Rev. E **95**, 023309 (2017).

[28] D. C. Marinescu, P. J. Weigele, D. M. Zumbühl, and J. C. Egues, Closed-Form Weak Localization Magnetoconductivity in Quantum Wells with Arbitrary Rashba and Dresselhaus Spin–Orbit Interactions, Phys. Rev. Lett. **122**, 156601 (2019).

[29] P. J. Weigele, D. C. Marinescu, F. Dettwiler, J. Fu, S. Mack, J. C. Egues, D. D. Awschalom, and D. M. Zumbühl, Symmetry breaking of the persistent spin helix in quantum transport, Phys. Rev. B **101**, 035414 (2020).

[30] A. A. Kiselev and K. W. Kim, Progressive suppression of spin relaxation in two-dimensional channels of finite width, Phys. Rev. B **61**, 13115 (2000).

[31] A. G. Mal'shukov and K. A. Chao, Waveguide diffusion modes and slowdown of D'yakonov–Perel' spin relaxation in narrow two-dimensional semiconductor channels, Phys. Rev. B **61**, R2413(R) (2000).

[32] A. W. Holleitner, V. Sih, R. C. Myers, A. C. Gossard, and D. D. Awschalom, Suppression of Spin Relaxation in Submicron InGaAs Wires, Phys. Rev. Lett. **97**, 036805 (2006).

[33] Th. Schäpers, V. A. Guzenko, M. G. Pala, U. Zulicke, M. Governale, J. Knobbe, and H. Hardtdegen, Suppression of weak antilocalization in $Ga_xIn_{1-x}As/InP$ narrow quantum wires, Phys. Rev. B **74**, 081301(R) (2006).

[34] Y. Kunihashi, M. Kohda, and J. Nitta, Enhancement of Spin Lifetime in Gate-Fitted InGaAs Narrow Wires, Phys. Rev. Lett. **102**, 226601 (2009).

[35] R. L. Kallaher, J. J. Heremans, N. Goel, S. J. Chung, and M. B. Santos, Spin and phase coherence lengths in n-InSb quasi-one-dimensional wires, Phys. Rev. B **81**, 035335 (2010).

[36] J. Wunderlich, B.-G. Park, A. C. Irvine, L. P. Zarbo, E. Rozkotov, P. Nemec, V. Novk, J. Sinova, and T. Jungwirth, Spin hall effect transistor, Science **330**, 1801 (2010).

[37] S. Z. Denega, T. Last, J. Liu, A. Slachter, P. J. Rizo, P. H. M. van Loosdrecht, B. J. van Wees, D. Reuter, A. D. Wieck, and

C. H. van der Wal, Suppressed spin dephasing for two-dimensional and bulk electrons in GaAs wires due to engineered cancellation of spin–orbit interaction terms, Phys. Rev. B **81**, 153302 (2010).

[38] J. Ishihara, M. Ono, Y. Ohno, and H. Ohno, A strong anisotropy of spin dephasing time of quasi-one-dimensional electron gas in modulation-doped GaAs/AlGaAs wires, Appl. Phys. Lett. **102**, 212402 (2013).

[39] P. Altmann, M. Kohda, C. Reichl, W. Wegscheider, and G. Salis, Transition of a two-dimensional spin mode to a helical state by lateral confinement, Phys. Rev. B **92**, 235304 (2015).

[40] J. Klinovaja and D. Loss, Parafermions in an Interacting Nanowire Bundle, Phys. Rev. Lett. **112**, 246403 (2014).

[41] Y. Oreg, E. Sela, and A. Stern, Fractional helical liquids in quantum wires, Phys. Rev. B **89**, 115402 (2014).

[42] A. Das, Y. Ronen, Y. Most, Y. Oreg, M. Heiblum, and H. Shtrikman, Zero-bias peaks and splitting in an Al–InAs nanowire topological superconductor as a signature of majorana fermions, Nat. Phys. **8**, 887 (2012).

[43] S. Heedt, N. Traverso Ziani, F. Crépin, W. Prost, St. Trellenkamp, J. Schubert, D. Grützmacher, B. Trauzettel, and T. Schäpers, Signatures of interaction-induced helical gaps in nanowire quantum point contacts, Nat. Phys. **13**, 563 (2017).

[44] A. Iorio, M. Rocci, L. Bours, M. Carrega, V. Zannier, L. Sorba, S. Roddaro, F. Giazotto, and E. Strambini, Vectorial control of the spin-orbit interaction in suspended InAs nanowires, Nano Lett. **19**, 652 (2019).

[45] M. Scheid, M. Kohda, Y. Kunihashi, K. Richter, and J. Nitta, All-Electrical Detection of the Relative Strength of Rashba and Dresselhaus Spin-Orbit Interaction in Quantum Wires, Phys. Rev. Lett. **101**, 266401 (2008).

[46] A. Sasaki, S. Nonaka, Y. Kunihashi, M. Kohda, T. Bauernfeind, T. Dollinger, K. Richter, and J. Nitta, Direct determination of spin–orbit interaction coefficients and realization of the persistent spin helix symmetry, Nat. Nanotechnol. **9**, 703 (2014).

[47] S. Faniel, T. Matsuura, S. Mineshige, Y. Sekine, and T. Koga, Determination of spin–orbit coefficients in semiconductor quantum wells, Phys. Rev. B **83**, 115309 (2011).

[48] K. Yoshizumi, A. Sasaki, M. Kohda, and J. Nitta, Gate-controlled switching between persistent and inverse persistent spin helix states, Appl. Phys. Lett. **108**, 132402 (2016).

[49] See Supplemental Material at http://link.aps.org/supplemental/10.1103/PhysRevB.103.094412 for detailed evaluation of the effective wire width, the weak antilocalization based on the Sawada model, and the expected value of the squared wave number along the growth direction.

[50] J. Nitta, T. Akazaki, H. Takayanagi, and T. Enoki, Gate Control of Spin–Orbit Interaction in an Inverted $In_{0.53}Ga_{0.47}As/In_{0.52}Al_{0.48}As$ Heterostructure, Phys. Rev. Lett. **78**, 1335 (1997).

[51] R. Landauer, Electrical resistance of disordered one-dimensional lattices, Philos. Mag. **21**, 863 (1970).

[52] M. Büttiker, Y. Imry, R. Landauer, and S. Pinhas, Generalized many-channel conductance formula with application to small rings, Phys. Rev. B **31**, 6207 (1985).

[53] M. Wimmer and K. Richter, Optimal block-tridiagonalization of matrices for coherent charge transport, J. Comput. Phys. **228**, 8548 (2009).